IEEE Photonics Journal
An IEEE Photonics Society Publication

Imaging Embryonic Stem Cell Dynamics Using Quantitative 3-D Digital Holographic Microscopy

Volume 3, Number 3, June 2011

A. Anand
V. K. Chhaniwal
B. Javidi, Fellow, IEEE

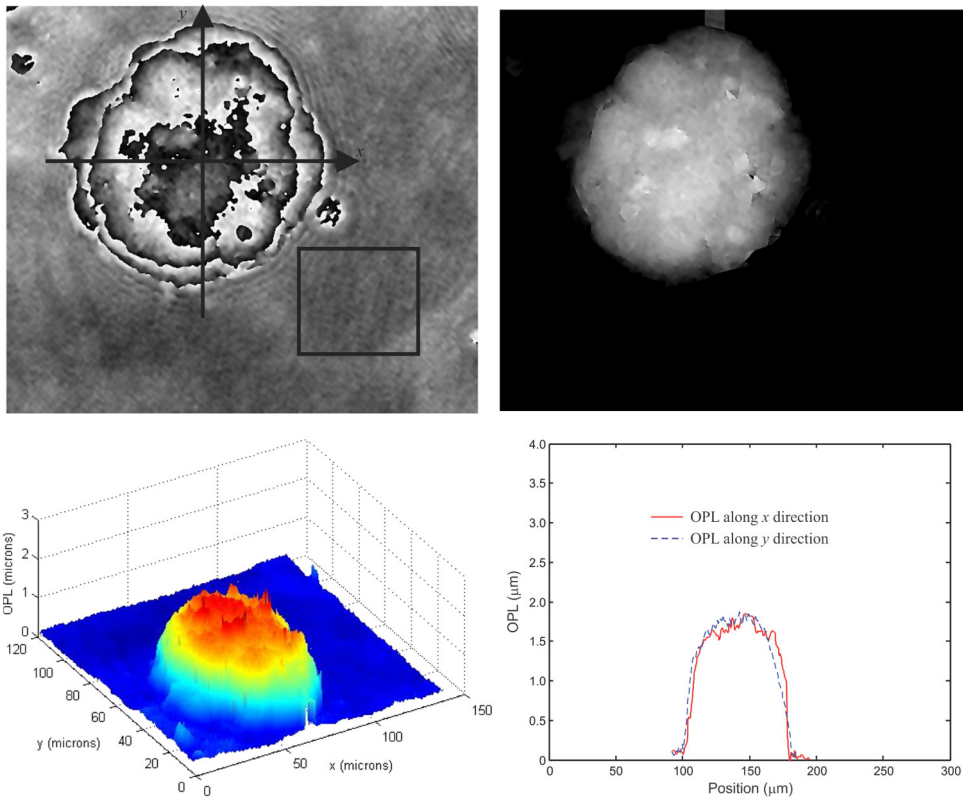

DOI: 10.1109/JPHOT.2011.2158637
1943-0655/$26.00 ©2011 IEEE

Imaging Embryonic Stem Cell Dynamics Using Quantitative 3-D Digital Holographic Microscopy

A. Anand,[1] V. K. Chhaniwal,[2,3] and B. Javidi,[4] *Fellow, IEEE*

[1]Applied Physics Department, Faculty of Technology and Engineering, The MS University of Baroda, Vadodara 390001, India
[2]Institut für Technische Optik, 70569 Stuttgart, Germany
[3]Applied Physics Department, Parul Institute of Engineering and Technology, Waghodia, Vadodara 391760, India
[4]Department of Electrical and Computer Engineering, U-2157, University of Connecticut, Storrs, CT 06269-2157 USA

DOI: 10.1109/JPHOT.2011.2158637
1943-0655/$26.00 ©2011 IEEE

Manuscript received May 27, 2011; accepted May 30, 2011.. Date of publication June 7, 2011; date of current version June 21, 2011. The work of V. K. Chhaniwal was supported by DST, Government of India under a Better Opportunities for Young Scientists in Chosen Areas of Science and Technology fellowship. The work of B. Javidi was supported by the Humboldt Foundation. Corresponding author: A. Anand (e-mail: arun_nair_in@yahoo.com).

Abstract: Embryonic stem cells are very important for the development of cell-based therapeutic strategies. Since stem cell colonies are nonpigmented and relatively transparent, they do not produce appreciable variation to the amplitude of probe electromagnetic radiation passing through them, necessitating the use of phase contrast imaging techniques for studying them. Here, we used digital holographic interferometric microscopy (DHIM) to observe temporal and spatial evolution of stem cell colonies. Three-dimensional or whole field imaging has yielded important quantitative information about their progression from single cell to colonies. Information on the time and spatial evolution of optical volume and path length change will be an important tool for biologists working in the area of stem cells and their development.

Index Terms: Imaging, microscopy, 3-D microscopy, holography, coherent imaging.

1. Introduction

The use of embryonic stem cells (ESCs) is wide ranging in treating diseases. Key to ESC evaluation is the ability to view cells in their various states of differentiation. However, currently no method is available to evaluate live cells in culture and determine their phenotype. The field of stem cell research desperately needs a means to characterize cells in culture as undifferentiated stem cells, fate-restricted progenitor cells, or differentiated mature cells. Most methods that are currently available require that the cells in culture are "fixed" with paraformaldehyde—killing the cells—so that specific proteins in the cell can be analyzed using antibodies with fluorescent tags for identification. Alternately, living cells in culture can be viewed using standard microscopy, but only gross morphology and not distinguishing characteristics can be evaluated. Another method relies on "cell sorting," which involves removing the cells from their growth conditions and passing them through a laser-guided "sorter" into a collection vial and then back to the Petri dish. Unfortunately, no method exists that allows full phenotypic evaluation of cultured ESCs without disrupting their established culture environment.

Microscopy provides the best method for imaging ESCs unintrusively, but the most challenging problem using bright field microscopy is in the imaging of semitransparent objects. Most of the

biological specimens, including ESCs, are transparent or semitransparent to visible radiation and do not have enough refractive index variation to produce appreciable change to the amplitude of the electromagnetic radiation passing through them. Therefore, it becomes very difficult to quantitatively image them with conventional bright field microscopy. The use of chemical staining becomes necessary to image such a specimen, but staining may produce an alteration to the cells or tissue and ultimately result in the destruction of the specimen. Also, the use of high magnification, high numerical aperture microscopic objectives (MOs) greatly reduces the depth of field of the imaged plane. Therefore, in conventional bright field microscopy, a mechanical movement of the objective lens (or the specimen) is required to focus on different object layers. Fortunately, however, the phase of the probe wavefront passing through such specimens is affected due to their nonuniform thickness or refractive index distribution. Phase contrast techniques use this phase change occurring to the probe wavefront for imaging transparent specimens. There are several methods in use in optical microscopy for imaging unstained specimens by converting the phase information to amplitude change; most common among them are Zernike and Nomarski methods [1]–[3]. However, to get quantitative information, one normally uses phase contrast techniques relying on optical interference. Most of the interferometric techniques use phase stepping to extract quantitative phase information, making them difficult to implement. With the advent of pixilated semiconductor arrays and fast, efficient computers, optical recording of holograms on such arrays and their numerical reconstruction became a reality, leading to the field of digital holography [4]–[7]. Numerical reconstruction of digitally recorded holograms by simulating the process of diffraction using scalar diffraction directly provides the complex amplitude of the object wavefront and, hence, the spatial phase distribution [4]. Digital holography also has the added advantage of numerical focusing, since each plane in the object has contributed to the hologram. Together, these properties make Digital Holography an attractive tool for imaging transparent and semitransparent biological specimens [8]–[20]. Since the numerical reconstruction yields the phase of the object wavefront, an interferometric comparison of the object phase distribution with any other phase distribution becomes possible. Therefore, by reconstructing the phase distribution with and without the object and then interferometrically comparing them, the distortions due to the aberrations in the optical system are removed. This leads to the field of digital holographic interferometric microscopy (DHIM). In this paper, the use of DHIM with angular spectrum propagation reconstruction for imaging dynamics of ESC colonies is described. To the best of our knowledge, this is the first time an attempt has been made to use digital holography as a quantitative evaluation tool for stem cell research.

2. Digital Holographic Interferometric Microscope

Fig. 1 depicts the schematic of the inverted digital holographic microscope used to study the dynamics of the ESC colony. The source used was a polarized He–Ne laser (max output power 15 mW, wavelength 632.8 nm). It was expanded and collimated and was split into two. One of these beams acts as the reference beam. The other beam passes through the object, and then, the MO $(20\times, \mathrm{NA} = 0.4)$ is placed below the object (making the setup inverted). The magnified object beam (probe beam) then interferes with the reference beam at the CCD (Prosilica, 8-bit, 4, 4μ pixel pitch) using a Mach–Zehnder setup. These interferograms (holograms) are recorded by the CCD and stored in a PC for numerical reconstruction.

Inverted setup allows use of large magnification, large numerical aperture, and short working distance microscope objectives without the need for immersion. The object was mounted on a translation stage, allowing easy focusing. In the present setup, the image plane was situated 150μ from the CCD plane. For each set of object holograms, a reference hologram (hologram without the ESC colony present) was also recorded for interferometric comparison.

3. Hologram Reconstruction

As discussed above, the recording of holograms digitally allows its reconstruction numerically. This is achieved by simulating the diffraction of the reference beam occurring at the microstructures of the recorded hologram using diffraction theory. Since the digitally recorded holograms are discrete

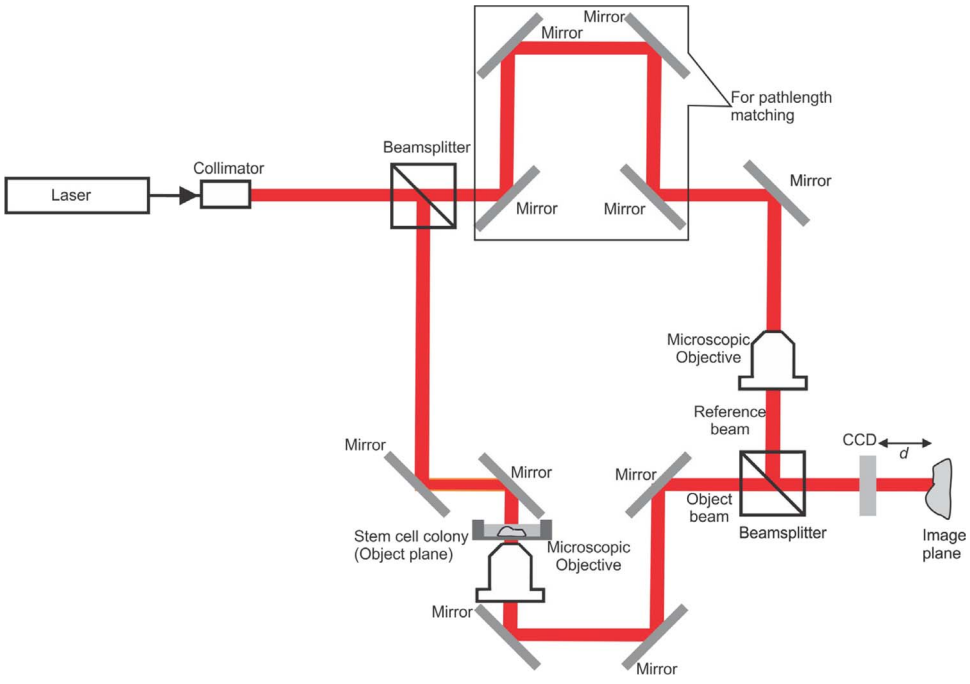

Fig. 1. Inverted digital holographic interferometric microscope for observation of ESC colonies.

in nature (finite pixel and array size), a discrete form of the diffraction integral is used. Depending upon the situation, the numerical reconstruction process can be based on either the Fresnel–Kirchhoff diffraction integral or the angular spectrum approach to the diffraction theory [4]. Both of these approaches describe the diffraction of the reconstructing reference wave at the microstructure of the hologram. For larger especially diffuse objects, the Fresnel–Kirchoff integral with Fresnel approximation is the appropriate approach to reconstruct the hologram, but in the present case, where transparent or phase objects are involved and propagation distances are short, an angular spectrum approach will be more appropriate. For microscopy of phase objects, the angular spectrum propagation approach also makes compact experimental setup possible. An added advantage of this method is that it can separate out the different diffracted beams in the frequency spectrum, and hence, there will not be overlap between any of the three beams in the reconstructions [14]. Reconstructions are achieved by propagating the filtered angular spectrum of the hologram illuminated by the reference beam.

The complex amplitude $U(x, y, 0)$ at the hologram plane $(x, y, 0)$ is obtained by illuminating the hologram (intensity distribution), which is a real number matrix, by the reference wave [14]

$$U(x, y; 0) = h(x, y)R(x, y) \tag{1}$$

where $h(x, y)$ is the hologram transfer function, and $R(x, y)$ is the complex reference wave. The Fourier transform of (1) provides its angular spectrum [21]

$$\hat{U}(f_X, f_Y; 0) = \int_{-\infty}^{\infty}\int U(x, y, 0)e^{-[i2\pi(f_X x + f_Y y)]}\, dx\, dy \tag{2}$$

with f_X, f_Y as the spatial frequencies in the x and y directions, respectively. Filtering is applied to the resulting spectrum so that the undiffracted reference beam and the conjugate real image are removed. By this filtering, the spectrum corresponding to the object alone can be selected. The

inverse Fourier transform of the filtered spectrum of (1) provides the modified complex amplitude at $(x, y, 0)$ containing information about the object alone [14]

$$\bar{U}(x, y, 0) = \int_{-\infty}^{\infty} \int filt\left[\hat{U}(f_X, f_Y; 0)\right] e^{i2\pi(f_X x + f_Y y)}\, df_X\, df_Y. \tag{3}$$

Here, *filt* represents the filtering of the angular spectrum. Complex amplitude at the image plane which is parallel to $(x, y, 0)$ plane and situated at a distance d from it is computed from the filtered spectrum using the free space propagation function and is given by [12]

$$U(x, y, d) = \int_{-\infty}^{\infty} \int \bar{U}(f_X, f_Y; 0) e^{ik\sqrt{1-\lambda^2 f_X^2 - \lambda^2 f_Y^2}\, d} e^{i2\pi(f_X x + f_Y y)}\, df_X\, df_Y. \tag{4}$$

The intensity of the object wavefront can be calculated from the complex amplitude given in (4) as

$$I(x, y) = |U(x, y)|^2. \tag{5}$$

The phase of the object wavefront is nothing but the angle the complex amplitude makes with the real axis and is

$$\phi(x, y) = \arctan \frac{\mathrm{Im}[U(x, y)]}{\mathrm{Re}[U(x, y)]}. \tag{6}$$

The phase of the probe wavefront with and without the object is computed individually from the complex amplitudes of the two reconstructed holograms states $U_O(x, y, t)$ and $U_R(x, y)$. Interferometric comparison (phase difference) provides information of the object alone at a particular time instance. The phases of the individual sates can be written as

$$\phi_O(x, y, t) = \arctan \frac{\mathrm{Im}[U_O(x, y, t)]}{\mathrm{Re}[U_O(x, y, t)]} \tag{7}$$

$$\phi_R(x, y) = \arctan \frac{\mathrm{Im}[U_R(x, y)]}{\mathrm{Re}[U_R(x, y)]}. \tag{8}$$

The interference phase (or phase difference) is now calculated directly by subtraction

$$\begin{aligned} \Delta\phi(x, y, t) &= \phi_O(x, y, t) - \phi_R(x, y), && \text{if } \phi_O > \phi_R \\ &= \phi_O(x, y, t) - \phi_R(x, y) + 2\pi, && \text{if } \phi_R > \phi_O. \end{aligned} \tag{9}$$

This phase difference acquired by a ray propagating in the z direction given in (9) is proportional to the optical path length (OPL) of the object at that time instance according to

$$\Delta\phi(x, y, t) = \frac{2\pi}{\lambda} \Delta n(x, y, t) L(x, y, t) \tag{10}$$

where $\Delta n(x, y, t)$ is the refractive index change between the exposures, and $L(x, y, t)$ is the thickness of the specimen. If the refractive index change is known, the physical thickness of the specimen can be determined; otherwise, the OPL $(\mathrm{OPL} = \Delta n \times L)$ of the specimen can be computed

$$\mathrm{OPL}(x, y, t) = \frac{\lambda \Delta\phi(x, y)}{2\pi}. \tag{11}$$

4. Computation of Various Physical Parameters of the Specimen

4.1. Lateral Dimension of the Specimen

Time evolution of the lateral size of the object under investigation sheds important information on its growth, as well as its interaction with its immediate surroundings. Lateral size can be directly obtained from the reconstructed 3-D profile (obtained from the OPL distribution).

4.2. Change in Maximum OPL

Maximum OPL provides information on the optical thickness of the specimen, and its time evolution will shed information on the axial growth of the specimen. This can be directly obtained from the path length distribution.

4.3. Area of the Specimen

A more important parameter will be the area of the specimen. It provides information on the lateral growth of the specimen. This can be directly computed from the OPL distribution. This is determined by first thresholding the obtained OPL with the mean path length where no specimen exists to obtain a binary image. After thresholding the number of pixels representing the specimen at the image plane is obtained and by multiplying this with the area each pixel occupies directly gives the area of the specimen. The area (A) each pixel occupies in the image plane is determined from the reconstructed pixel size (which is equal to camera pixel size Δx and Δy when Angular Spectrum Propagation (ASP) integral is used for reconstructions) and lateral magnification (M) of the system

$$A = \frac{\Delta x \Delta y}{M}. \tag{12}$$

4.4. Optical Volume of the Specimen

Time evolution of the optical volume of specimen under consideration will provide information on its overall growth. Optical volume of the specimen at any time instance is determined from the optical height distribution and area each pixel occupies (A) in the image plane. Since the obtained optical height distribution is discrete, volume can be determined from

$$V(t) = A \sum_{k} \sum_{l} \mathrm{OPL}(k, l, t). \tag{13}$$

5. Experimental Results

R1-669 mouse ESCs (a gift from J. Rossant, University of Toronto) were maintained on a mitomycinC-treated E13.5 mouse fibroblast feeder layer in DMEM (Invitrogen) with 15% fetal calf serum (FBS, HyClone), 2 mM glutamax (Invitrogen), 1 mM sodium pyruvate (Invitrogen), 0.1 mM nonessential amino acids (Invitrogen), 0.55 mM 2-mercaptoethanol and leukemia inhibitory factor (1000 U/mL), and penicillin–streptomycin–neomycin (Invitrogen). Prior to imaging, ESCs were treated with trypsin for passaging and seeded onto glass slides (LabTek II, Nunc). Holograms of the ESC colonies were obtained at 24-h intervals for 4 days, starting on the second day of culture. These holograms were used to compute the OPL distribution of the ESC colony at each time instance. The ESC container was put back in the incubator after imaging. To make sure that the same colony was imaged, the outside of the container was marked at the position it was imaged. Fig. 2(a) shows the obtained wrapped phase distribution for a day-2 colony of ESCs after interferometric comparison with the reference hologram (hologram recorded without the cell colony but with the medium containing the cell colonies). Fig. 2(b) is the unwrapped phase map, which is used for determination of OPL distribution. The area marked by the rectangle was used to determine the

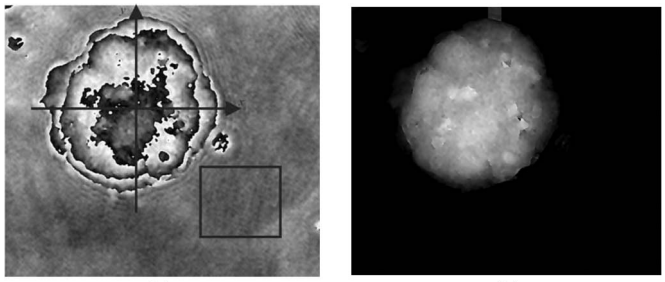

(a) (b)

Fig. 2. (a) Wrapped phase map for a day-2 ESC colony. (b) Unwrapped phase distribution using Goldstein's branch cut method.

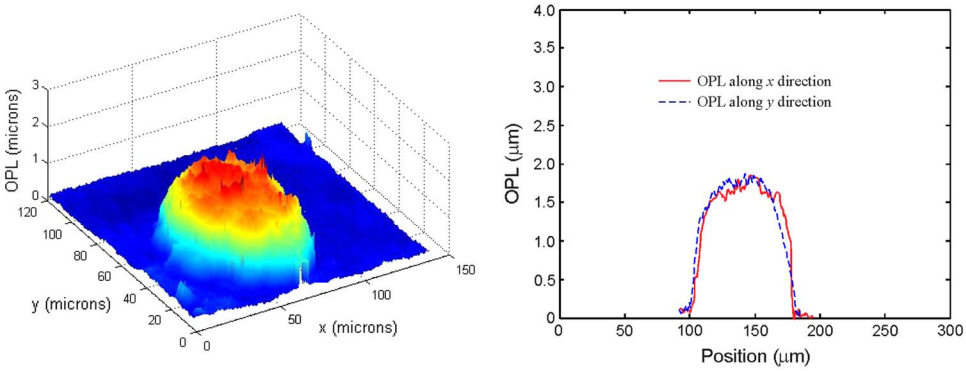

(a) (b)

Fig. 3. (a) Three-dimensional OPL distribution of the ESC colony computed from the unwrapped phase distribution shown in Fig. 2(b). (b) Path length variation along the *x* and *y* direction shown in Fig. 2(a).

error in determination of OPL. This error arises due to the inherent phase variations in the system. The mean standard deviation using all the phase maps was less the 1.2 nm. Fig. 3 shows the 3-D OPL distribution of the colony after 2 days. From Fig. 3(b), it can be see that the colony is almost spherical. The area of the ESC colony was determined after thresholding OPL distribution with the mean OPL in the area where there is no cell. The threshold image is shown in Fig. 4. The computed area is 3.27×10^{-8} m^2. Fig. 5(a) shows wrapped phase distribution obtained for a day-3 colony of ESCs. The unwrapped phase distribution is shown in Fig. 5(b). From Fig. 5(a) and (b), the fibroblast cells delivering nutrients to the ESCs can be clearly seen (indicated by the rectangle), and it can be seen that the fibroblast cell optical height is based on individual cells and is therefore very small compared with that of the ESC colony OPL height in which multiple ESCs pile on top of each other. The maximum OPL, lateral dimensions, area, and volume are computed from the reconstructed OPL profile.

From Fig. 5, it can be seen that the colony expands more in the *y* direction. The maximum path length, as well as area and volume, also increase, indicating more stem cells coming to the colony. Fig. 6 shows the change in the OPL distribution for day-4 and day-6 ESC colony. From Figs. 2(b), 3(c), and 6(a) and (b), it can be deduced that the colony expands laterally and axially, indicating the incorporation of more cells (or division of cells) into the colony.

Fig. 7 summarizes the obtained physical parameters from the quantitative phase contrast imaging of ESC colonies.

It can be summarized that the axial growth of the colony exponentially increases after day 4. The change in the lateral size along the *y* direction is almost linear with time. The change in area and

Fig. 4. Binary image used for area calculation obtained after thresholding Fig. 2(b).

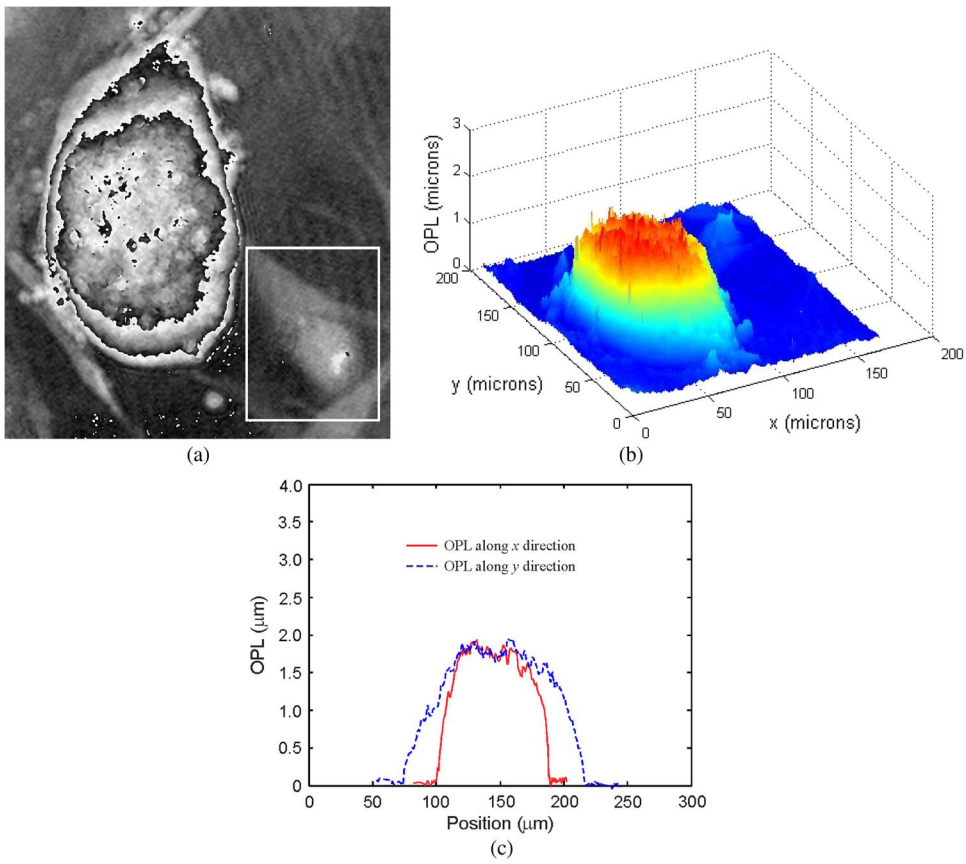

Fig. 5. (a) Obtained wrapped phase distribution and (b) 3-D OPL distribution for a day-3 colony. (c) Optical profile along *x* and *y* directions.

volume gives similar profile. They start to increase rapidly after day 3. It indicates rapid lateral and axial expansion of the colony.

6. Conclusion

Rigorous control of stem cell differentiation is important for all regenerative medicine applications using stem cells. This proposed 3-D visualization and measurement approach can be used to

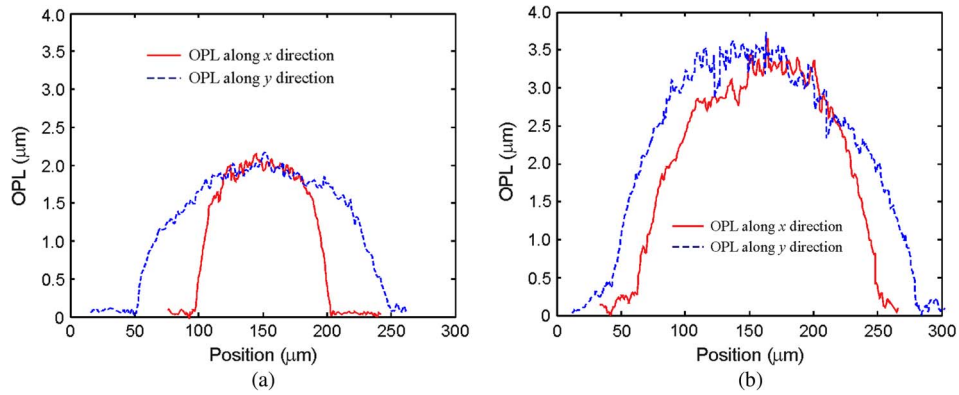

Fig. 6. (a) Optical profile along *x* and *y* directions for a day-4 and (b) day-5 ESC colony.

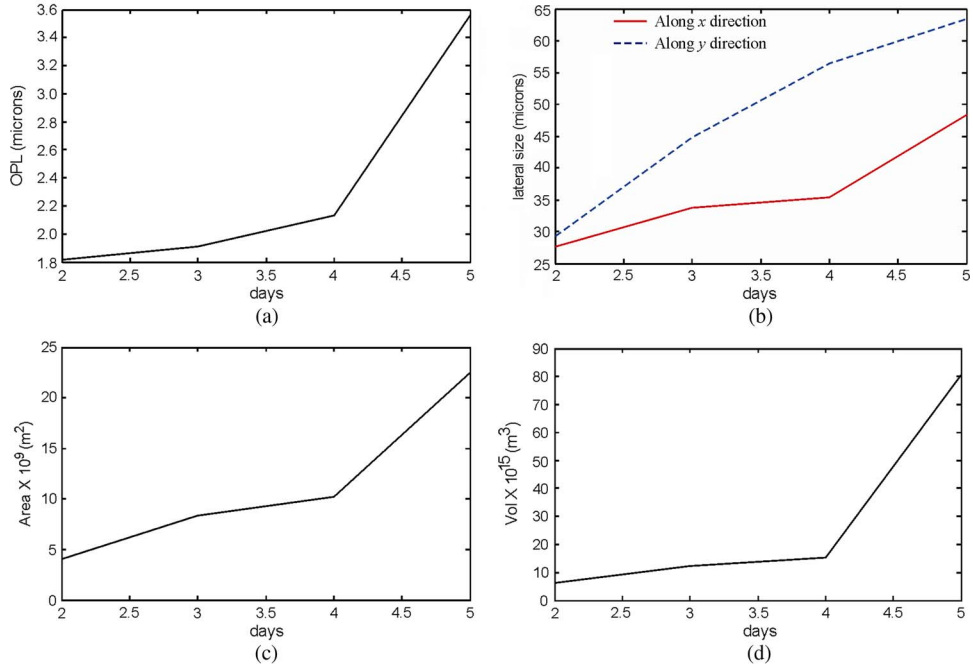

Fig. 7. Time evolution of various parameters. (a) Maximum OPL, (b) lateral size, (c) area, and (d) volume of the stem cell colony.

analyze details of ESC and monitor their profiles throughout the differentiation process and the cell proliferation rate. DHIM was found to work well with the 632.8 nm He–Ne source. Since the exposure to the imaging radiation was very low (due to small power and lower exposure times), it can be assumed that the damage to the cells is negligible, but this needs to be investigated further. Another alternative will be to use an infrared source which has negligible absorption coefficient for living cells. Even though it may reduce the lateral resolution of the system, it will cause less radiation damage.

The proposed 3-D imaging and visualization technique using DHIM can be used to identify the ideal conditions for efficient stem cell self-renewal and ultimately mature differentiated cells. It can be made into an *in situ* quantitative imaging technique for stem cell research for real-time imaging of the cell as well as colony growth. It can also be used for automatic sorting of different cells using statistical algorithms. Further research is progressing in this direction.

Acknowledgment

The authors wish to acknowledge Prof. J. Conover and J. Lennington of the University of Connecticut, for providing the stem cell samples and helpful discussions, and Dr. M. Daneshpanah of GE Global Research for helpful suggestions and remarks. V. K. Chhaniwal would like to thank DST, Govt. of India for support under Better Opportunities for Young Scientists in Chosen Areas of Science and Technology (BOYSCAST) fellowship. B. Javidi acknowledges support from the Humboldt Foundation.

References

[1] M. Martinez-Corral and G. Saavedra, "The resolution challenge in 3D optical microscopy," *Progr. Opt.*, vol. 53, pp. 1–67, 2009.
[2] D. B. Murphy, *Fundamentals of Light Microscopy and Electronic Imaging*. New York: Wiley-Liss, 2001.
[3] F. Zernike, "Phase contrast, a new method for microscopic observation of transparent objects," *Physica*, vol. 9, no. 7, pp. 686–698, Jul. 1942.
[4] U. Schnars and W. Jueptner, *Digital Holography: Digital Hologram Recording, Numerical Reconstruction and Related Techniques*. Berlin, Germany: Springer-Verlag, 2005.
[5] U. Schnars and W. Jueptner, "Digital recording and numerical reconstruction of holograms," *Meas. Sci. Technol.*, vol. 13, no. 9, pp. R85–R101, Sep. 2002.
[6] T. Kreis, Ed., *Handbook of Holographic Interferometry*. New York: Wiley, 2005.
[7] J. W. Goodman and R. W. Lawrence, "Digital image formation from electronically detected holograms," *Appl. Phy. Lett.*, vol. 11, no. 3, pp. 77–79, Aug. 1967.
[8] T. Zhang and I. Yamaguchi, "Three-dimensional microscopy with phase-shifting digital holography," *Opt. Lett.*, vol. 23, no. 15, pp. 1221–1223, Aug. 1998.
[9] B. Kemper, A. Bauwens, A. Vollmer, S. Ketelhut, P. Langehanenberg, J. Müthing, H. Karch, and G. von Bally, "Label-free quantitative cell division monitoring of endothelial cells by digital holographic microscopy," *J. Biomed. Opt.*, vol. 15, 036009, 2010.
[10] E. Cuche, F. Bevilacqua, and C. Depeursinge, "Digital holography for quantitative phase-contrast imaging," *Opt. Lett.*, vol. 24, no. 5, pp. 291–293, Mar. 1999.
[11] P. Marquet, B. Rappaz, P. J. Magistretti, E. Cuche, Y. Emery, T. Colomb, and C. Depeursinge, "Digital holographic microscopy: A noninvasive contrast imaging technique allowing quantitative visualization of living cells with subwavelength axial accuracy," *Opt. Lett.*, vol. 30, no. 5, pp. 468–470, Mar. 2005.
[12] I. K. Moon, M. Daneshpanah, A. Stern, and B. Javidi, "Automated three-dimensional identification and tracking of micro/nano biological organisms by computational holographic microscopy," *Proc. IEEE J.*, vol. 97, no. 6, pp. 990–1010, Jun. 2009.
[13] Y. Frauel, T. Naughton, O. Matoba, E. Tahajuerce, and B. Javidi, "Three dimensional imaging and display using computational holographic imaging," *Proc. IEEE J.*, vol. 94, no. 3, pp. 636–653, Mar. 2006.
[14] A. Anand, V. Chhaniwal, and B. Javidi, "Real-time digital holographic microscopy for phase contrast 3D imaging of dynamic phenomena," *IEEE J. Disp. Technol.*, vol. 6, no. 10, pp. 500–505, Oct. 2010.
[15] B. Javidi, I. Moon, S. Yeom, and E. Carapezza, "Three-dimensional imaging and recognition of microorganism using single-exposure on-line (SEOL) digital holography," *Opt. Exp.*, vol. 13, no. 12, pp. 4492–4506, Jun. 2005.
[16] P. Ferraro, S. Grilli, D. Alfieri, S. De Nicola, A. Finizio, G. Pierattini, B. Javidi, G. Coppola, and V. Striano, "Extended focused image in microscopy by digital Holography," *Opt. Exp.*, vol. 13, no. 18, pp. 6738–6749, Sep. 2005.
[17] F. Dubois, L. Joannes, and J.-C. Legros, "Improved three-dimensional imaging with digital holography microscope using a partial spatial coherent source," *Appl. Opt.*, vol. 38, no. 34, pp. 7085–7094, Dec. 1999.
[18] G. Pedrini and H. J. Tiziani, "Short-coherence digital microscopy by use of a lensless holographic imaging system," *Appl. Opt.*, vol. 41, no. 22, pp. 4489–4496, Aug. 2002.
[19] B. Javidi and E. Tajahuerce, "Three dimensional object recognition using digital holography," *Opt. Lett.*, vol. 25, no. 9, pp. 610–612, May 2000.
[20] A. Anand and B. Javidi, "Three dimensional microscopy with single beam wavefront sensing and reconstruction from volume speckle fields," *Opt. Lett.*, vol. 35, no. 5, pp. 766–768, Mar. 2010.
[21] J. W. Goodman, *Introduction to Fourier Optics*. New York: McGraw-Hill, 1996.